Journal of Materials Chemistry B

ROYAL SOCIETY OF CHEMISTRY

PAPER

View Article Online
View Journal | View Issue

Cite this: *J. Mater. Chem. B*, 2026, **14**, 2014

Systematic investigation of the effects of neural stem cell spheroid size and density on fate specification in 3D culture

Rebecca Duquette, Sabrina Pietrosemoli Salazar, Ze Zhong Wang, Alireza Sohrabi and Stephanie K. Seidlits

Received 16th August 2025,
Accepted 12th January 2026

DOI: 10.1039/d5tb01589h

rsc.li/materials-b

A systematic understanding of how the density of neural stem/progenitor cells (NS/PCs) embedded within three-dimensional (3D) biomaterials affect cell behavior will be necessary for developing effective strategies to generate CNS tissues. Here, we investigated the effects of local and global cell density of mouse neural stem cells (mNSCs) on their viability, proliferation, and differentiation when cultured in 3D, hyaluronic acid (HA)-based hydrogel matrices. Specifically, we assessed the influence of spheroid size, which represents local cell density, (small: 100 cells per sphere, large: 200 cells per sphere) and seeding density (low: 100 000 cells per hydrogel, high: 200 000 cells per hydrogel), which represents global density, on cellular outcomes. Results reveal that these factors have both independent and interactive effects on NS/PC viability and fate. Cultures of smaller spheres at low global densities yield more glial cells, including astrocytes and oligodendrocytes. In contrast, cultures with high global densities, regardless of sphere size, better preserved stem-like mNSC phenotypes. Strikingly, cultures with 1000 total spheres per hydrogel, regardless of sphere size or overall cell concentration, best maintained viability while promoting neuronal maturation. These findings highlight the importance of controlling both local and global cell densities in 3D cultures to achieve reproducible mNSC-derived populations for use as *in vitro* test beds or biomanufacturing of therapeutic stem cells.

Introduction

Neurodegenerative diseases involve progressive deterioration of the brain and spinal cord tissues that comprise the central nervous system (CNS). Alzheimer's and Parkinson's diseases are the most prevalent, estimated to affect around 7 million people as of 2024[1] and 1 million people as of 2020,[2] respectively, in the United States. Traumatic injuries to the brain and spinal cord also cause significant losses of CNS tissue and function, affecting approximately 5.3 million people in 2025[3] and 308 620 people in 2024,[4] respectively, in the United States. Despite the vast numbers of people affected by loss of CNS functions, no current treatments can regenerate these tissues once lost, motivating the widespread efforts from the research and medical communities to develop new therapies. Stem cell-based therapies offer substantial promise for CNS repair, particularly given the limited regenerative capabilities of CNS tissues following injury or neurodegeneration. However, success has been limited by poor survival and inefficient engraftment of transplanted cells.[5] Besides use as tissue grafts, stem cells can be used to create *in vitro* models of human neurodegenerative disease and injury which researchers can use to identify and evaluate new, promising drug therapies. Re-creation of neural tissues, either *in vitro* or *in vivo*, will likely require precise control over stem cell maturation within three-dimensional (3D), tissue-like environments.

3D hydrogel scaffolds, which can be designed to have similar water content, biochemical composition, and mechanical properties as native CNS tissues, have emerged as useful platforms for cultivating neural stem/progenitor cells (NS/PCs) that can facilitate their maturation into physiologically equivalent neuronal networks.[5–7] Furthermore, cells can be embedded within a 3D hydrogel matrix to provide a more *in vivo*-like microenvironment that better supports survival and maturation of NS/PCs in culture and enables inclusion of higher densities of NS/PCs than can 2D monolayers, which better approximate the dense neuronal networks present in the native CNS.[8] Hyaluronic acid (HA) is a glycosaminoglycan that interacts with transmembrane receptors to effect NS/PC proliferation, differentiation and maturation in the CNS extracellular matrix (ECM) and the subventricular zone, which persists as a neural stem cell niche throughout adulthood.[9] HA-based hydrogels can be mechanically tuned to approximate CNS tissue

The University of Texas at Austin Biomedical Engineering (BME), 107 W Dean Keaton St., Austin, TX 78712, USA

elasticity, where softer materials tend to improve NS/PC survival, differentiation and the ability of mature neural cells to extend neurites.[10–12] HA-based hydrogels have been shown to reliably support *in vitro* 3D culture of NS/PCs and can also be an effective delivery vehicle for cell transplants due to their good injectability, stability, biodegradability, and biocompatibility.[7,10,13,14]

Encapsulating NS/PCs in 3D biomaterials as spheroids or aggregates, as opposed to single cells, leads to increased adhesion, survival, ECM deposition and more consistent differentiation.[15,16] Compared to single cells, spheroids experience increased cell–cell interactions leading to a secretome rich in paracrine signals and retained secreted matrix within a 3D biomaterial.[17] In general, spheroids have an inherent gradient of oxygen, nutrients and metabolites which leads to a necrotic core region, surrounded by viable, but quiescent cells and a peripheral layer of proliferating cells, especially when greater than 300 μm.[18–21] In contrast to single cells in 3D biomaterial culture in which spontaneous differentiation has been observed, spheroid culture better preserves stemness and multipotency until placed under specific medium formulation protocols to induce directed differentiation.[22,23] N-cadherin, and subsequent β-catenin activation, has been linked to improved stem cell maintenance.[24,25] Depending on the cell and biomaterial scaffold choices that are relevant for a study, it can be difficult to tightly control spheroid size due to limitations of spheroid formation methods and loss of aggregate cohesiveness during the encapsulation process due to physical mixing of the biomaterial scaffold.[26] Previous research has indicated a correlation between spatial distribution of spheroids within 3D biomaterials and cell sprouting, migration, and inter-sphere fusion, highlighting the nuanced effects of spheroid crosstalk on cell responses.[27] Consistent evidence across cell types and culture platforms has indicated that sphere size plays a critical role in viability, proliferation and differentiation of encapsulated cells. A global density of NSCs in the range of 1–2 × 106 cells per mL within 3D biomaterial scaffolds has been shown to promote viability and neuronal differentiation in previous studies.[28,29] However, it remains unclear how multiple neural cell-based spheroids will interact in dense culture within a 3D scaffold.

In the current study, we evaluated how NS/PC spheroid size and overall cell density affect NS/PC survival and differentiation potential, through independently tuning spheroid size and density within a 3D biomaterial. Specifically, we investigated mouse neural stem cell (mNSC) spheroids cultured within hyaluronic acid (HA)-based, 3D hydrogels that were matched to the HA content and elastic modulus of the native CNS. Previously, our group has demonstrated that HA-based hydrogels with these specifications can support 3D culture and differentiation of NS/PCs.[10] This study adds to our previous findings by characterizing how spheroid size and overall cell density could be used to control mNSC viability and fate. Results from these studies are expected to guide cell-level choices when developing future CNS therapeutics.

Experimental

Materials and methods

HA-based hydrogel formation. Hyaluronic acid (700 kDa, LifeCore Biomedical) was prepared using carbodiimide chemistry (*N*-hydroxysuccinimide, NHS: 1-ethyl-3-(30dimethylaminpropyl), to add thiol groups from cystamine (Sigma-Aldrich) to the carboxylic acid of the glucuronic acid of the HA monomers. Dithiothreitol (DTT) was then used to break disulfide bridges leaving free thiol groups and the HA-SH backbone was purified using dialysis (12–14 kDA molecular weight cellulose membrane, Spectrum Labs) over a period of 72 hours to remove excess DTT to purify the HA-SH which was then sterilized and lyophilized for 48 hours. Proton nuclear magnetic resonance (H-NMR) spectroscopy and Ellman's reagent (5,5′-dithiobis-(2-nitronebzoic acid), Sigma Aldrich) according to Gold Biotechnology Ellman's Test Protocol, were used to assess the percent thiolation for each batch of HA-SH. HA was modified in batches to achieve a range of thiolation (4.5–6.0 ± 0.5%). HA-SH was combined with thiol-terminated, 4-arm polyethylene glycol (PEG-SH, 20 kDa, Laysan Bio) to achieve target amounts of total moles of thiol, pH adjusted to 6.5 and reacted with maleimide-terminated, 4-arm polyethylene glycol (PEG-Mal, 20 kDa, Laysan Bio) at a 1 : 1.2 ratio using Michael-type addition. An RGD containing peptide (GCGYGRGDSPG) or L-cysteine hydrochloride monohydrate (Millipore Sigma, C6852-25G) was incorporated into each hydrogel at a final concentration of 270 μm. Cylindrical silicone isolator molds (GRACE Bio-Labs, 4.5 mm, 664206, or 9 mm diameter, 664201, 1 mm depth) were autoclaved, cooled, dried and placed into the bottom of 24-well plates. Equal quantities of HA and crosslinker solutions were mixed within each mold and the well plate was placed in a bead bath (37 °C) for 30 minutes to fully form. The silicone rubber molds were then carefully removed, leaving the hydrogels within the wells. For 3D cell culture, a total hydrogel volume of 20 μL was used in the 3 mm diameter molds. In contrast a total volume of 80 μL in the 9 mm diameter molds were used for rheological characterization, as hydrogels must be size matched to the parallel-plate geometry used. Dulbecco's phosphate-buffered saline (PBS) was added to each well, then the well plate was wrapped with Parafilm and stored at 4 °C overnight. For cell encapsulation into the HA-based hydrogels, the same protocol was followed except that everything was maintained in a sterile environment, and the hydrogels were formed in 4.5 mm silicone isolator molds and hydrogels were maintained in a 48-well plate for the duration of culture.

Rheological characterization of hydrogels. After overnight swelling in PBS, hydrogels were evaluated for viscoelastic properties using a discovery hybrid rheometer (DHR2) from TA instruments. Hydrogels were brought to room temperature and placed onto the bottom plate of the rheometer which was heated to 37 °C. A parallel-plate geometry (9 mm) was used to perform an oscillation-frequency logarithmic sweep (0.1–10 Hz, 1.0% strain). Complex moduli were recorded and used to calculate averages and standard deviations of 5 technical replicates.

Cell culture. Cryopreserved mouse spinal cord neural stem cells (mNSCs) (E15-18, C57/Bl6) were purchased from Millipore Sigma (SCR031) and used at passage 2 or 3 for all experiments. mNSCs were thawed and expanded in culture on poly-L-ornithine (PLO)/laminin-coated flasks to have a large enough population for encapsulation into the hydrogels. On day 0, cells were counted and plated into AggreWell™400 (STEMCELL Technologies, 34415) plates, that were first coated with 5% Pluronic F127, at either 100 or 200 cells per microwell. They were then cultured in these plates with proliferation medium (0.02 μg mL^{-1} epidermal growth factor (Fisher Scientific, AF10015100), 0.02 μg mL^{-1} basic fibroblast growth factor (ThermoFisher Scientific, 100-18B-100UG), 2 μg mL^{-1} heparin (Millipore Sigma, H6279-25KU) and 0.2× ABAM (Millipore Sigma, A5955-20 mL) in basal medium (Millipore Sigma, SCM003)) for 48 hours in an incubator (37 °C, 5% CO_2). On day 2, the spheres were taken up from the AggreWell™400 plates and encapsulated into 20 μL HA-based hydrogels. The encapsulated spheres within the hydrogels were then cultured in differentiation medium (1 μM Retinoic Acid (Millipore Sigma, R2625-50 mg), 5 μM Forskolin (Millipore Sigma, F3917-10 mg), 0.2× ABAM (Millipore Sigma, A5955-20 mL) in basal medium (Millipore Sigma, SCM003)) for five days in an incubator (37 °C, 5% CO_2) with media changes every other day.

Cell viability. After 5 days of culture in differentiation medium, viability was assessed using a TUNEL viability assay (Thermo Fisher Scientific, C10619), which uses a fluorescent label to tag fragmented DNA, an indicator of apoptosis. Hydrogels were embedded and sectioned before the assay was applied. Fluorescent images were taken, and image quantification was performed to obtain a quantitative measurement of relative viability. Additionally, a Live/Dead assay (Abcam ab115347), which labels live cells green and dead cells red, was performed on hydrogels after 24 hours of culture to qualitatively assess relative viability of the small and large sphere sizes at the higher global density using fluorescence microscopy.

Cell proliferation. After 5 days of culture in differentiation medium, the hydrogels were incubated at 1 : 1000 with EdU Staining Proliferation Kit (iFluor 647) (abcam, ab222421), for one and a half hours in an incubator (37 °C, 5% CO_2). EdU (5-ethynyl-2′-deoxyuridine), is a thymidine analog which is incorporated into newly synthesized DNA by cells within a sample over a controlled period. A fluorescent azide can then be added and covalently cross-link to the EdU in a 'click' chemistry reaction. Measuring newly synthesized DNA is the most accurate way to measure DNA proliferation. After this incubation period they were washed with PBS to remove the EdU solution and then incubated at 1 : 1000 with LIVE/DEAD™ Fixable Green Dead Cell Stain Kit (ThermoFisher Scientific, L23101), for thirty minutes in an incubator (37 °C, 5% CO_2). This dye reacts with free amines in both the interior of cells with compromised membranes and on the cell surface of cells. After the incubation period, the hydrogels were washed with 1% bovine-serum albumin (BSA) (Millipore Sigma, A9418-50G) in PBS, twice. Then cells were extracted from the hydrogels first by 5-minute incubation in Tryple™ Express Enzyme (Fisher Scientific, 12-604-021) while vortexing to break the cells away from the hydrogels, then using the GentleMACS Tissue Dissociator system to break up the spheres into single cells. The Umbilical Cord Dissociation Kit (Miltenyi Biotec, 130-105-737) was used for the 1-hour dissociation period at 37 °C. After dissociation, cells were washed, fixed and permeabilized. Next the EdU additive solution was added to conjugate the fluorophore to the EdU and was incubated at room temperature for 30 minutes. Cells were then washed twice and kept on ice until flow cytometry. As a negative control for EdU measurements, one tube of cells that had been grown on 2D substrates alongside hydrogels did not receive EdU but did receive incubation with the fluorescence click chemistry reagent. This control group was assessed with flow cytometry to (1) identify autofluorescent background signal and assign a minimum threshold over this value and (2) identify signal from single cells compared to cell debris or cell clusters. Additionally, a positive control for dead cells was prepared prior to flow cytometry using a 15-minute incubation of cells with 70% EtOH, which will cause many cells to die. Cells were then filtered and transferred to 12 × 75 mm flow tubes. They were analyzed on a flow cytometer (ThermoFisher Scientific, Attune NxT) at E_x/E_m = 495/520 nm (LIVE/DEAD) and E_x/E_m = 649/664 nm (EdU). The LIVE/DEAD signal was analyzed first to determine the population of living cells. This assay yields two peaks of fluorescence signal that typically have a 50-fold difference between them and relates to the presence of live *vs.* dead cells. The percentage of proliferating cells was then calculated from the living population.

Embedding and sectioning. On the fifth day of culture, hydrogels were fixed overnight at 4 °C (4% paraformaldehyde), embedded (Tissue-Plus OCT Compound Fisher Scientific 23-730-571) into cryomolds and stored at -80 °C. Hydrogel blocks were then sectioned on an Avantik® QS12 Cryostat. Cryosections (10 μm thick) were collected from the center region of the hydrogel cylinder onto positively charged microscope slides.

Immunostaining and imaging. Immunostaining was performed on 10 μm-thick cryosections of hydrogels from non-overlapping sections to represent distinct areas and spheres within the hydrogels. Immunostaining for TUNEL, Ki-67, SOX2, βIII-tubulin, NeuN, GFAP and RIP was performed to assess overall viability, proliferation, stemness and differentiation of mNSCs (Table S1). Sections were labeled according to location in the hydrogel and fixed with 4% paraformaldehyde onto the positively charged microscope slides. Next, they were rinsed (3 × five minutes) with PBS-Tween (0.05%), permeabilized with PBS-Triton (0.1%), if applicable for the antibody, and then rinsed again (3 × five minutes). Blocking solution was prepared, 4% Normal Donkey Serum (Sigma-Aldrich D9663), 2% bovine serum albumin (Spectrum Chemical 22070008) and two drops of M.O.M blocking agent (Vector Laboratories, MKB-2213-1) in PBS-Tween (0.05%) and added to each section of the slide. This was left for an hour at room temperature, then the slides were rinsed again with PBS-Tween (3 × five minutes) and the primary antibody solutions were added (Table S2).

Slides were stored overnight at 4 °C and the next day the secondary antibody solutions were added (Table S2). Slides were then mounted with coverslips using Fluoromount G (Fisher Scientific, OB100-01), dried for half an hour, sealed with clear nail polish and stored at 4 °C until imaging. Images were acquired on a Zeiss Axio Observer 7 microscope using Zen2 software (Zeiss) and an ORCA-Flash4.0V.2 CMOS (Hamamatsu) camera (20× air 0.55 NA objective). Negative controls, which did not receive primary antibody, were also imaged. All slides from the independent repeats were stained and imaged at the same time to minimize variability. Thus, images were acquired using constant exposure times for each antibody across all conditions.

Image analysis. Data collected include quantification of images from 3 hydrogel cultures that were performed independently (different NSC batches) with 3–4 images (randomly sampled, non-overlapping regions within the hydrogel, each image covers ~0.3 mm^2, 20× objective) per hydrogel. This resulted in each condition having 9–12 total images (individual data points on graph) per condition per statistical assessment. In the graphs, individual data points shown indicate a single image taken from a hydrogel culture. Image analysis was performed using the open-source software CellProfiler. The pipeline first converted each channel to binary (gray) images. Then a watershed function was applied to the former blue channel (Hoescht) and the locations were stored. For nuclear markers (*e.g.*, TUNEL, Ki-67, SOX2, and NeuN), the average diameter of objects was measured and then used to set the bounds for primary object identification of the relevant channel. The location of primary objects (nuclear stain) was then related to the locations of nuclei to create a new related object (*i.e.*, nuclear stained cells). Then these objects were counted and divided by the total nuclei count to give a percentage of nuclear expression. For protein markers with non-nuclear expression (*e.g.*, βIII-tubulin, GFAP and RIP), the total area of positive staining was calculated by applying a global threshold and measuring the are occupied by the relevant channel (pixels). It was necessary to take a global area measurement because the cells were densely packed, making it difficult to accurately relate the non-nuclear marker expression with a specific cell. The number of pixels per μm^2 was then calculated and used to convert number of $pixels^2$ to μm^2. Then this total area (μm^2) was divided by the total number of nuclei to give area of expression (μm^2) per number of nuclei.

Statistical analyses. GraphPad Prism 10 was used to create data plots and for statistical analyses. For any images that looked markedly different from the others, a ROUT outlier analysis (Q = 1%) was applied to identify outliers. After removing these outliers, a Shapiro–Wilk normality test was performed (α = 0.05). An ordinary two-way ANOVA was then run with a Tukey's multiple comparison test (α = 0.05) to assess significant differences between the experimental conditions and variation due to group effects.

Results and discussion

Here we highlight how local and global cell density and emergently total number of spheres in an HA-based hydrogel affects viability, proliferation and differentiation of encapsulated NSCs. This research demonstrates that total number of spheres within a 3D biomaterial platform plays an equally important role to that of sphere size and should be tightly controlled when drawing conclusions about the effects of biomaterial scaffolds on encapsulated cells.

Sphere sizes are roughly uniform when encapsulated for 3D matrix culture

To generate consistently sized mNSC spheroids, either 100 or 200 cells were cultured in Aggrewell™ plate suspension (no matrix) for 48 hours in proliferation medium prior to encapsulation in hydrogels for 3D culture (Fig. 1a). Spheroid size was measured immediately before encapsulation (Fig. 1b). The average diameter (124 ± 11 μm) of spheres formed using 100 cells was significantly smaller than the average diameter (146 ± 13 μm) of the spheres formed using 200 cells (Fig. 1c). Phase and Live(green)/Dead(red) fluorescence (Fig. 1d) images were taken after 24 hours of culture within the hydrogels to provide a qualitative assessment of spheroid distribution and viability of the small and large spheres at a high global density within the hydrogels.

HA was used as the base for the hydrogels in this study given its abundance and role as a polymeric backbone in the CNS ECM and ability to interact with NS/PCs *via* the CD44 receptor. Our group has previously reported that HA concentration and hydrogel shear modulus can be independently tuned to determine the behavior of cultured cells.[10,30] The biomaterials used for this study were fabricated using high molecular weight (~700 kDa) and 0.5 (w/v%) HA to best approximate the HA content in the native CNS.[31] Furthermore, the shear modulus of these hydrogels was selected to approximate that of brain tissue (~200 Pa).[32,33] Finally, we included an RGD-bearing peptide that can interact with integrins on cultured cells to promote adhesion to the 3D hydrogel matrix.

HA-based hydrogels, 0.5% w/v HA, 201 ± 11 Pa complex modulus (Fig. S1), were then seeded at either a low (100 000 cells per hydrogel) or high (200 000 cells per hydrogel) global density. The global density can be divided by the number of cells per sphere to give a measure of total number of spheres in a single hydrogel (Table 1). Based on these results, reproducible spheroid sizes can be achieved for encapsulation at specific global densities within the 3D hydrogels. This approach provides a robust method to interrogate the effects of both sphere size and global density of cells within a hydrogel platform independently.

Highest viability was observed in conditions with 1000 total spheres

Viability of small and large 3D matrix-embedded spheroids was assessed after 5 days of culture in differentiation medium using a TUNEL assay, which fluorescently labels nicked DNA. Two-way ANOVA showed that sphere size had the biggest effect on apoptosis ($p < 0.0005$, Table S3). Global density also had a significant effect ($p < 0.005$, Table S3) and the interaction between the two variables showed the greatest significance ($p < 0.0001$, Table S3). Post-hoc, pairwise analyses confirmed

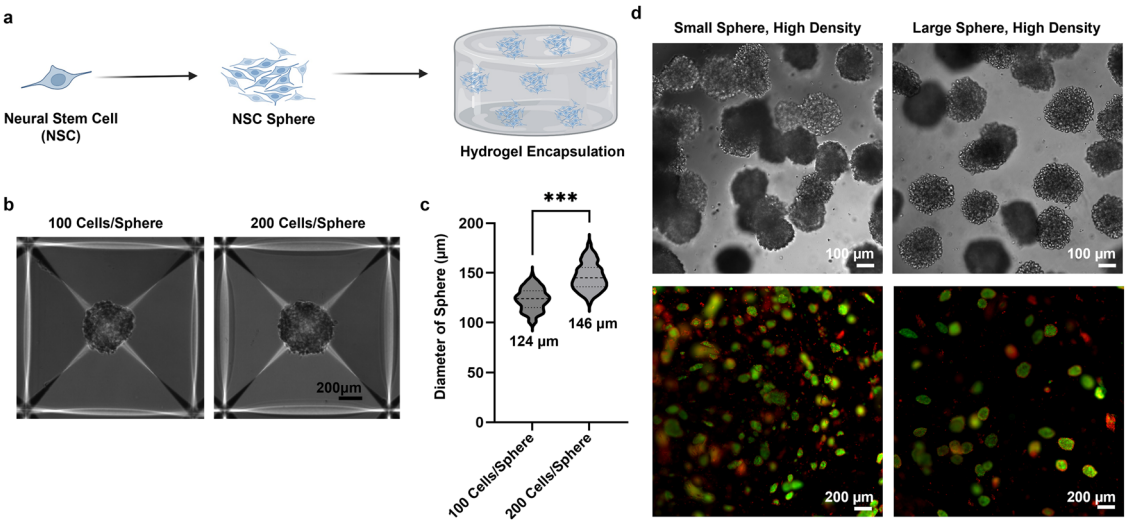

Fig. 1 (a) Overview schematic of the encapsulation process for spheres into hyaluronic acid-based hydrogels. NSC spheroids of small (100 cells) or large (200 cells) size were encapsulated at one of two global densities, either low (100 000 cells per hydrogel) or high (200 000 cells per hydrogel). (b) Phase contrast images of the spheres within the AggreWell™ plate. Scale bar is 200 μm. (c) Averaged diameters were calculated and plotted (N = 72 spheres, 1 independent preparation, error bars show ± SD). A two-tailed, unpaired t-test was performed to determine statistical difference (***$p < 0.001$). (d) (top) Phase contrast images of the small and large spheres within the hydrogels at a high global density. Scale bar is 100 μm. (bottom) LIVE (green)/DEAD (red) images of the small and large spheres within the hydrogels at a high global density. Scale bar is 200 μm.

Table 1 Sphere size, global density, global concentration and total number of spheres for each condition in the study

Condition	Sphere size	Global density	Global concentration	Total number of spheres
Small sphere, high desnity	100 cells per sphere	200 000 cells per hydrogel	2 million cells per mL	2000
Small sphere, low density	100 cells per sphere	100 000 cells per hydrogel	1 million cells per mL	1000
Large sphere, high density	200 cells per sphere	200 000 cells per hydrogel	2 million cells per mL	1000
Large sphere, low density	200 cells per sphere	100 000 cells per hydrogel	1 million cells per mL	500

that the small spheres (*i.e.*, 100 cells) spheres cultured at higher densities (*i.e.*, 200 000 cells per hydrogel) had significantly more apoptotic cells than all other conditions (Fig. 2b). The two 1000 total sphere conditions had significantly fewer apoptotic cells than the other two total sphere conditions (*i.e.*, 500 and 2000), indicating that the total sphere number has the greatest effect on the viability of cultures in a 3D matrix environment. This study demonstrates that even smaller spheroids that do not have necrotic cores (<300 μm diameter) and within the range of global cell density (1–2 × 106 M cells per mL) known to support NS/PC growth,[28,29,34] viability can be hindered by total sphere density within a 3D matrix. The increased apoptotic activity observed in the 2000 total spheres per hydrogel condition may be attributed to inadequate availability of nutrients and oxygen at this highest local cell density.[35] When cells, including NSCs, undergo apoptosis they release reactive oxygen species (ROS),[36] which can induce death of neighboring cells[37] Conversely, ROS levels are significantly elevated when cells are seeded in monolayers at densities lower than 1×10^5 cells per cm^2, leading to poor viability of several cell types, including NSCs.[38] In the current study, for 3D cultures with 500 total spheres embedded in a 20 μL, cylindrical hydrogel with a 4 mm diameter, the cross-sectional area of the hydrogel is 12.5 mm^2, translating to a spheroid density of ~40 spheres per mm^2 and a cell density (assuming the larger, ~150 μm diameter spheres with 200 cells each) around 8×10^5 cells per cm^3. Thus, we suspect that this lower cell density interferes with necessary paracrine and other cell–cell interactions.

Small spheres at the lower global density were more proliferative than cells at the high global density regardless of sphere size

Proliferation was assessed *via* nuclear expression of Ki-67 after five days of culture in differentiation medium (Fig. 3a–c). Global density had a significant effect on the percentage of Ki-67-positive cells ($p < 0.05$, Table S3). While there was no significant effect of sphere size, two-way ANOVA indicates a significant interactive effect of sphere size and global density ($p < 0.05$). Post-hoc, pairwise comparisons showed that the small spheres seeded at the lower density group had significantly more nuclear expression of Ki-67 than the small spheres seeded at the higher density ($p < 0.05$). No other significant differences were found. These findings indicate that 3D cultures at higher cell densities, either local (*i.e.*, sphere size) or global, are less proliferative. A previous result found that NSC/NPC proliferation is upregulated when cultured in 3D in spheroids or aggregates (75–175 μm diameter), compared to in 2D monolayer cultures.[34] However, they reported a steady

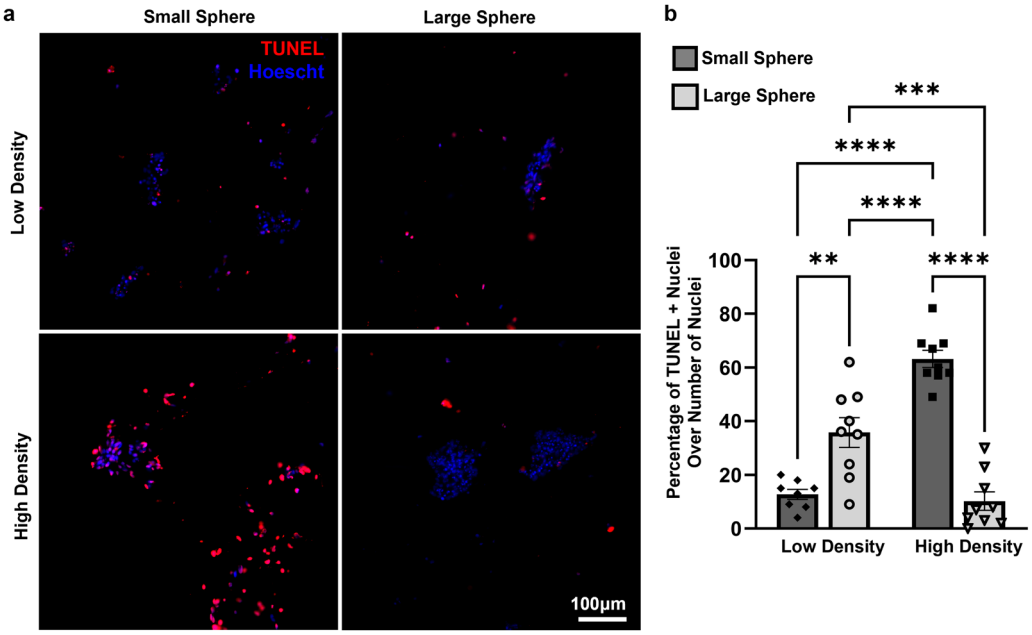

Fig. 2 On day 5 of culture in differentiation medium, the hydrogels were fixed, sectioned at 10 μm and (a) a TUNEL assay was performed alongside nuclear staining, Hoescht, to confirm the presence of apoptotic cells. Scale bar is 100 μm. (b) These images were analyzed using cell profiler to determine the percentage of nuclear expression (**$p < 0.01$, ***$p < 0.001$, ****$p < 0.0001$, $N = 9$, error bars represent ± SEM). A test of normality (Shapiro–Wilk test) and subsequently ordinary two-way ANOVA (Tukey's multiple comparison test) was performed using GraphPad Prism to determine significance difference between the groups. The small sphere, high density group had a higher proportion of TUNEL expression than all other groups indicating it had the poorest viability. The large sphere, low density group had a higher proportion of TUNEL expression than the small sphere, low density and large sphere, high density groups.

decrease in doubling times with increasing spheroid diameters up to around 250 μm before reaching a constant doubling time for spheroids with 250–400 μm diameters,[34] likely due to increasing oxygen gradients that restrict proliferation to the periphery of the sphere.[18] Thus, given the spheroid sizes used in this study, were maintained between 110–160 μm, it is not surprising that differences in global density had a stronger influence on proliferation than spheroid size. Since sphere size alone did not affect proliferation, the relatively poor proliferation in the 2000 spheres per hydrogel condition compared to the 1000 spheres per hydrogel condition may instead be due to similar mechanisms to those posited for the poor viability in this condition. For example, the release of ROS that occurs after neural cell death has been correlated with a reduction in proliferation and sphere size.[39] A future direction of this work could be to measure the changes in sphere size and production of ROS over time in this densely packed condition to better understand the underlying changes that affect both viability and proliferation.

Separately, flow cytometry was used to measure relative fluorescence from the conditions after an EdU assay which relates the proportion of cells that have actively divided (*i.e.*, underwent S phase) during the assay period (90 min) (Fig. 3d). No significant effects of sphere size or global density were detected by two-way ANOVA. The EdU data indicate that about 10% of the population actively divided during the 90-minute assay period. In contrast, nuclear Ki-67 is expressed in the nucleus during all active phases of the cell cycle (G1, S, M, G2) and, thus, is expected to identify a higher percentage of cycling cells than the EdU assay (around 40–60% *versus* 10–20%, respectively). The Ki67+ cells observed likely reflected cells that proliferated earlier than day 5 of culture as the mNSCs became adapted to the differentiation medium and mitogen withdrawal.

Numbers of SOX2-positive NSCs were similar across all conditions

mNSCs were maintained for five days in differentiation medium before assessing nuclear expression of SOX2, a transcription factor that is critical for maintaining the self-renewal and pluripotency of NSCs (Fig. 4). Statistical analysis indicated a significant effect of global cell density on numbers of SOX2-positive cells ($p < 0.05$, Table S3), with the lower global density producing a larger $Sox2^+$ population. However, no significant differences were observed from post-hoc, pairwise comparisons. Despite increased numbers of proliferative cells in the small spheroid, low cell density condition, there do not appear to be more pluripotent stem cells in this condition. Instead, both Ki-67 and SOX2 were expressed in about 40% of mNSCs across the board, even in differentiation medium which lacks mitogens. While SOX2-postive stem cells are typically proliferative,[40] co-localization of Ki67 and SOX2 was not evaluated in this study, so we cannot say for certain that the SOX2 and Ki67 were expressed by the same mNSCs.

Neuronal differentiation was maximized in cultures seeded with 1000 spheroids

Differentiating neurons were identified by the presence of βIII-tubulin, a marker of both immature and mature neurons, and

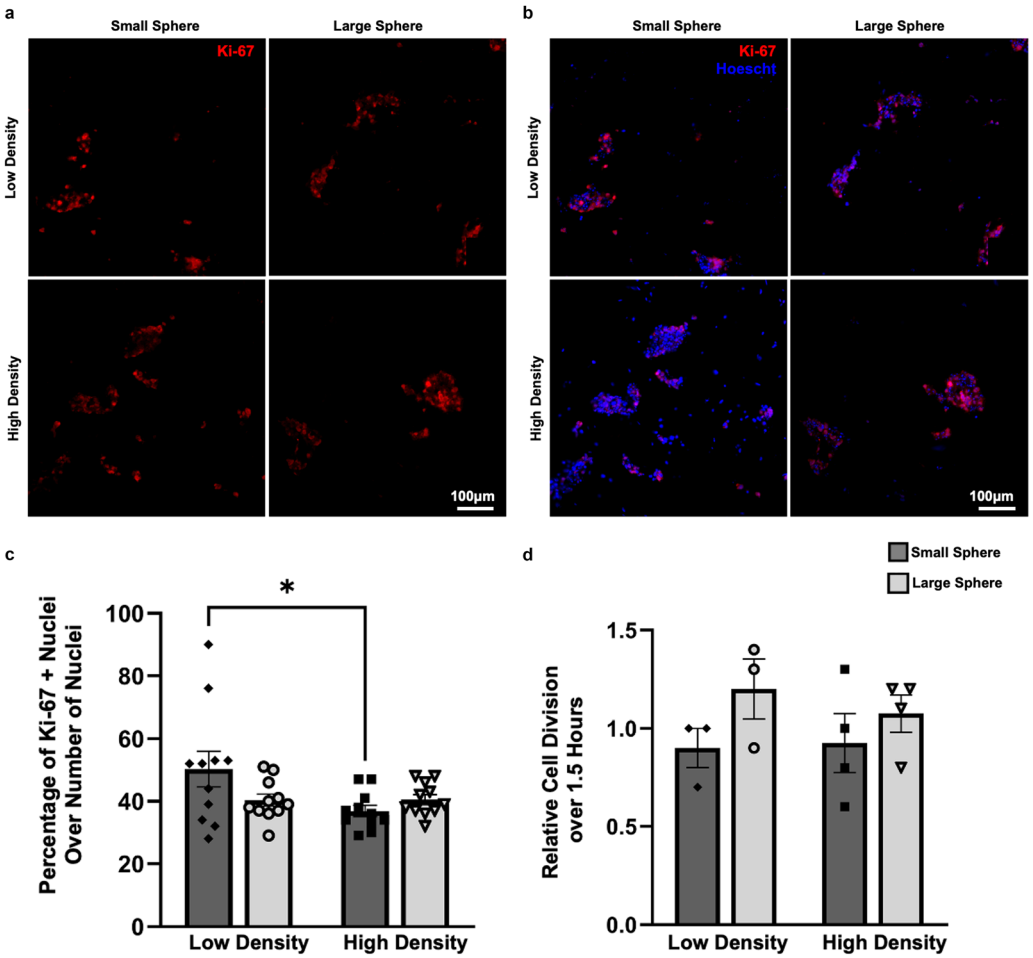

Fig. 3 On day 5 of culture in differentiation medium, the hydrogels were fixed, sectioned at 10 μm and stained for (a) Ki-67 and (b) Ki-67 with Hoescht to confirm the presence of proliferative cells. Scale bars are 100 μm. (c) These images were analyzed using cell profiler to determine the percentage of nuclear expression (*$p < 0.05$, $N = 11$, error bars represent ± SEM). A test of normality (Shapiro–Wilk test) and subsequently ordinary two-way ANOVA (Tukey's multiple comparison test) was performed using GraphPad Prism to determine significance difference between the groups. The small sphere, low density group had a higher proportion of nuclear Ki-67 expression than the small sphere, high density group. (d) Flow cytometry was performed to compare proliferation, represented by the percentage of EdU positive cells. A test of normality (Shapiro–Wilk test) and subsequently ordinary two-way ANOVA (Tukey's multiple comparison test) was performed using GraphPad Prism to determine significance between the groups. ($N = 3$–4, error bars represent ± SEM). No significant differences were observed.

NeuN, a nuclear protein present in mature neurons (Fig. 5a–d). The βIII-tubulin-positive area was normalized by the number of nuclei in each respective image (Fig. 5e). There were statistically significant effects of both sphere size ($p < 0.0005$) and global density ($p < 0.0001$) as well as an interactive effect ($p < 0.0001$) (Table S3). Pairwise comparison shows that the small sphere, high density condition had significantly lower expression of βIII-tubulin expression than all other conditions ($p < 0.0001$). While there were no significant independent effects of either sphere size or cell density on NeuN expression, there was a significant interaction observed ($p < 0.005$, Table S3). There were no statistically significant differences between groups found during post-hoc, pairwise analyses. However, conditions with 1000 total spheres (Table 1) had a non-statistically significance trend associating higher NeuN expression than the lower and higher total sphere conditions (500 and 2000 spheres per hydrogel, respectively).

Together, these findings clearly show that both sphere size and global cell density affect neuronal differentiation and indicate that total spheres per culture may be a more direct way to control generation of neurons. The clearest observation was that the highest spheroid density (2000 spheres per hydrogel) promoted the least immature and mature neurons (βIII-tubulin$^+$), potentially due to nutrient competition between the individual spheroids. Moreover, it suggests that there may be an optimal condition for promoting neuronal differentiation in which cell density is high enough to support robust paracrine signaling while remaining low enough to support adequate nutrient and waste exchange. No significant differences were observed when comparing NeuN expression across groups, as there was marked variability in individual cultures across independent repeats (Fig. 5f). Interestingly, some 3D cultures exhibited extensive NeuN expression, which others had very little expression. This variability could be to the manual mixing

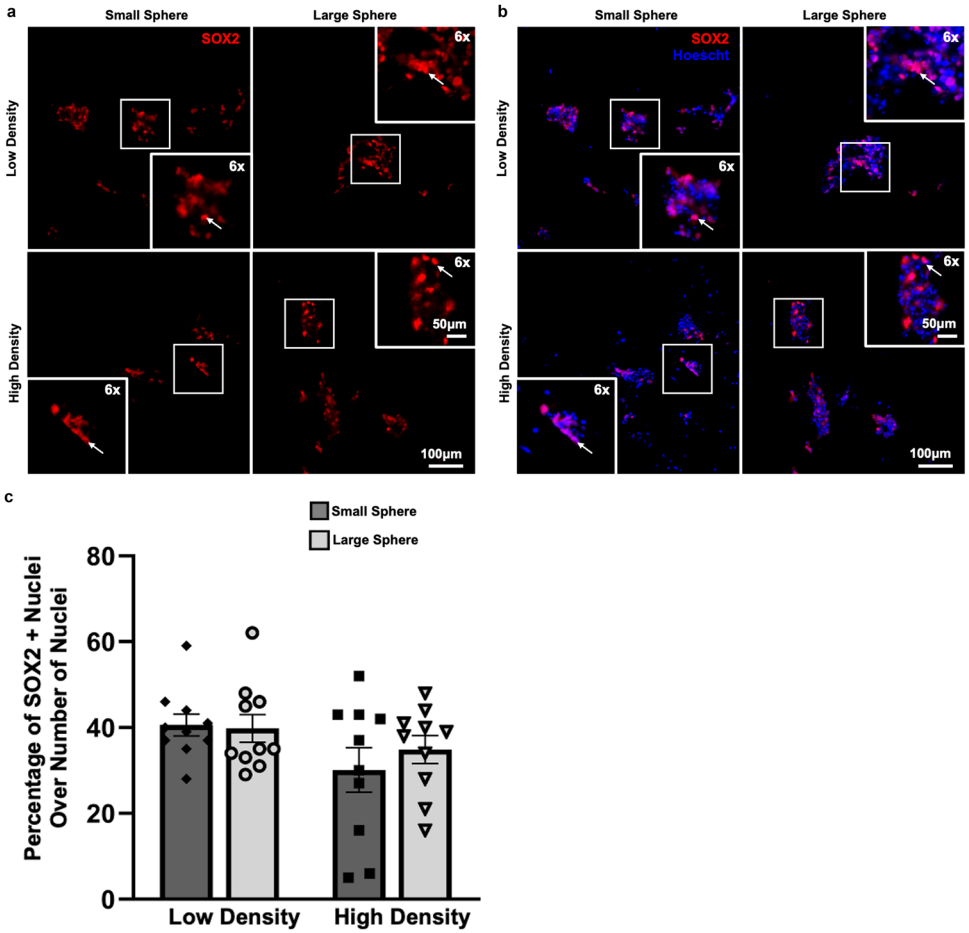

Fig. 4 On day 5 of culture in differentiation medium, the hydrogels were fixed, sectioned at 10 μm and stained for (a) SOX2 and (b) SOX2 with Hoescht to confirm the presence of stemlike cells. Scale bars are 100 μm, inset scale bar is 50 μm. (c) These images were analyzed using cell profiler to determine the percentage of nuclear expression of SOX2 (N = 10, error bars represent ± SEM). A test of normality (Shapiro–Wilk test) and subsequently ordinary two-way ANOVA (Tukey's multiple comparison test) was performed using GraphPad Prism to determine significance difference between the groups. There were no significant differences observed between the groups. However, there was a group effect observed, indicating that global density was a source of variation (*$p < 0.05$).

of spheroids into the hydrogels leading to uncontrolled distances between the spheroids.[41] Previous research has shown that, 100 μm diameter spheroids of NSCs encapsulated into hydrogels had increased proliferation and neuronal differentiation after 7 days in culture compared to single, dispersed NSCs[42] Combining a tight range of small sphere size (100–125 μm) with a low global density (1 M cells per mL), and thus a 1000 total sphere density, in a way that better controls sphere placement throughout the hydrogel may further improve neuronal differentiation beyond what was observed in this research. Additionally, it may be that some NSCs in the spinal cord-derived population would require additional time to mature into NeuN-expressing neurons so that differences would become more apparent.

Lower global density cultures were enriched in GFAP-positive astrocytes

Mouse NSCs differentiating into astrocytes were identified by expression of GFAP, an astrocyte-specific intermediate filament protein (Fig. 6a). The GFAP-positive area was normalized by the number of nuclei in each respective image for quantification (Fig. 6b). Global density ($p < 0.0001$), but not sphere size, had statistically significant independent effects on GFAP expression (Table S3). However, there was also a significant interaction effect of global density and sphere size ($p < 0.05$). In post-hoc, pairwise comparisons, the low global density, small sphere condition had significantly higher GFAP expression than both the small ($p < 0.001$) and large sphere ($p < 0.01$) conditions at the high global density. Additionally, the low global density, large sphere condition had significantly more GFAP expression than the high global density, small sphere condition ($p < 0.01$) and to a lesser extent the high global density, large sphere condition ($p < 0.05$). In general, astrocytes upregulate GFAP under stress,[43] so it is possible that reduced paracrine support in the low global density conditions initiates a stress response in differentiating glia. While GFAP expression is commonly used to identify astrocytes, not all astrocytes will express GFAP. Thus, it is possible that there are astrocytes with less reactive

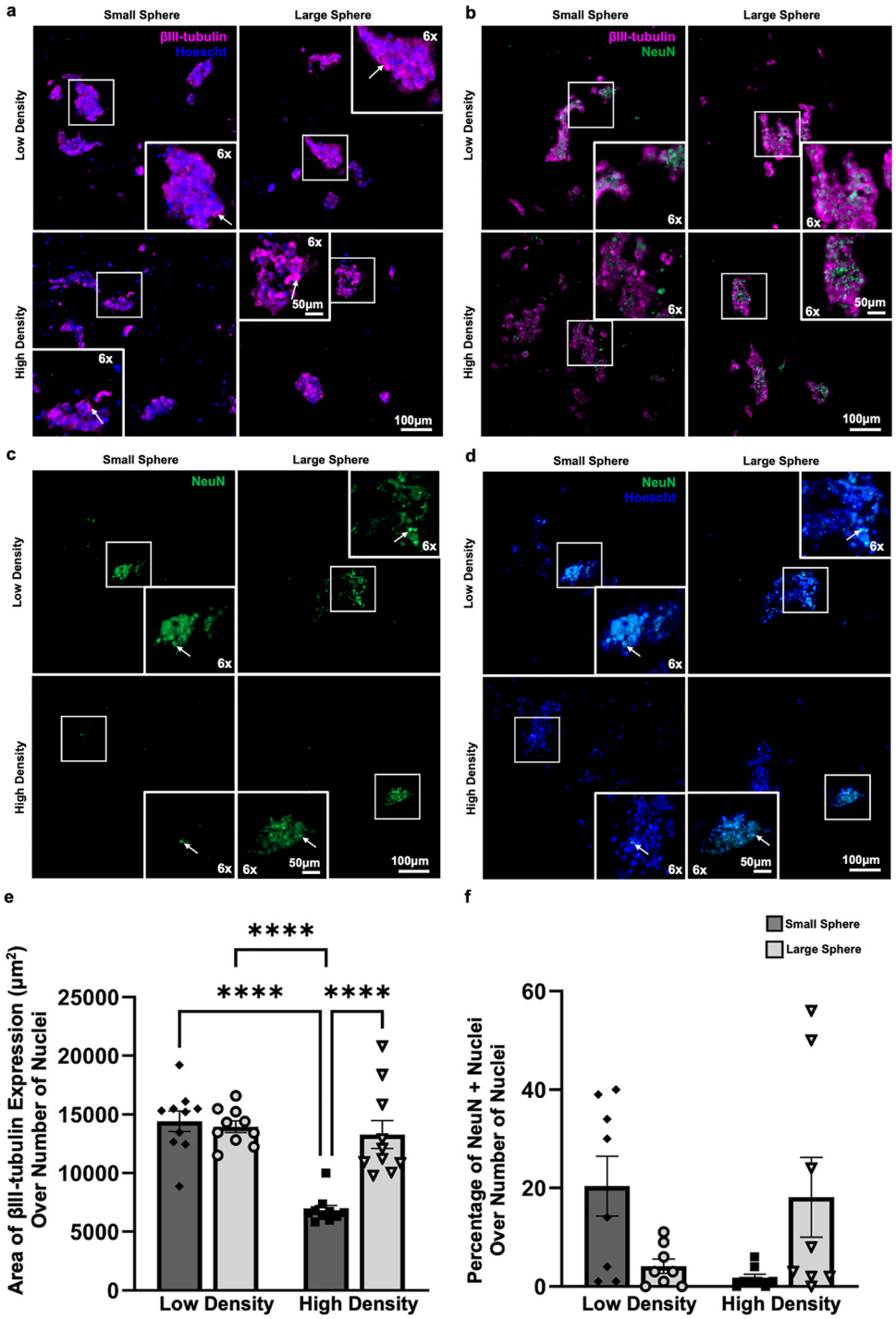

Fig. 5 On day 5 of culture in differentiation medium, the hydrogels were fixed, sectioned at 10 μm and stained for (a) βIII-tubulin and Hoescht to confirm the presence of immature neuronal cells. Scale bars are 100 μm, inset scale bar is 50 μm. (b) Sections were then co-stained for βIII-tubulin and NeuN to observe overlap of the two markers. Scale bars are 100 μm. (c) Separate sections were also stained for NeuN and (d) NeuN with Hoescht to confirm the presence of mature neuronal cells. Scale bars are 100 μm. (e) Images were analyzed using cell profiler to determine the total area of expression of βIII-tubulin divided by the number of nuclei. A test of normality (Shapiro–Wilk test) and subsequently ordinary two-way ANOVA (Tukey's multiple comparison test) was performed using GraphPad Prism to determine significance between the groups. (****$p < 0.0001$, $N = 10$, Error bars represent ± SEM). The small and large sphere, low density and large sphere, high density groups had a higher amount of expression than the small sphere, high density group. (f) Images were analyzed using cell profiler to find the percentage of nuclear expression of NeuN ($N = 8$, error bars represent ± SEM). A test of normality (Shapiro–Wilk test) and subsequently ordinary two-way ANOVA (Tukey's multiple comparison test) was performed using GraphPad Prism to determine significance between the groups. There were no significant differences between the groups, however there was a significant interaction factor (**$p < 0.005$) between sphere size and global density.

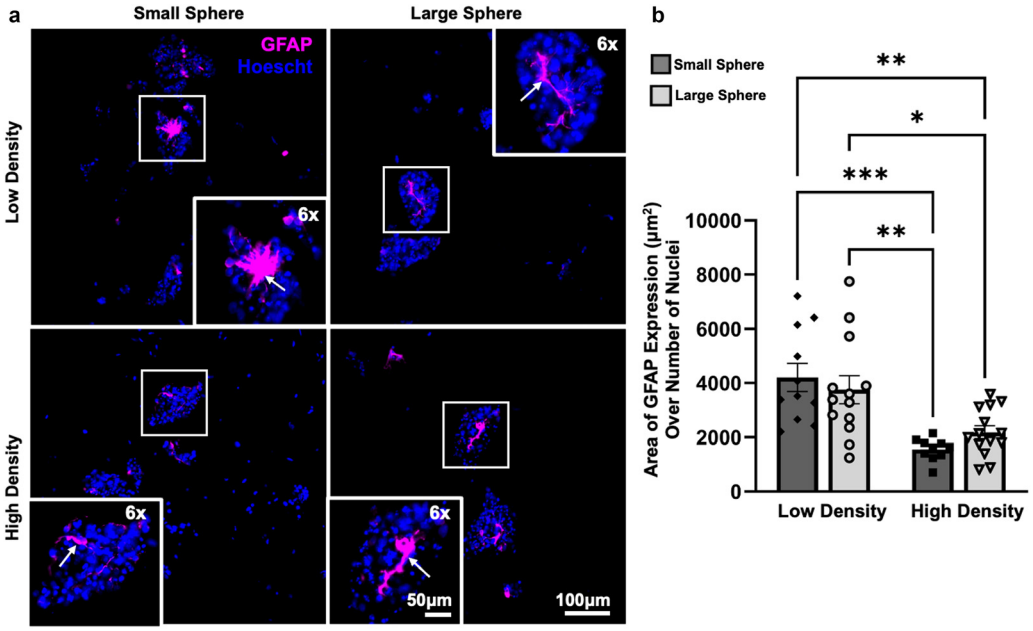

Fig. 6 On day 5 of culture in differentiation medium, the hydrogels were fixed, sectioned at 10 μm and stained for (a) GFAP and Hoescht to confirm the presence of astrocytes. Scale bar is 100 μm, inset scale bar is 50 μm. (b) These images were analyzed using cell profiler to determine the total area of expression divided by the number of nuclei. A test of normality (Shapiro–Wilk test) and subsequently ordinary two-way ANOVA (Tukey's Multiple comparison test) was performed using GraphPad Prism to determine significance between the groups. (*$p < 0.05$, **$p < 0.01$, *** $p < 0.001$, $N = 10$, Error bars represent ± SEM). The small sphere, low density group had a higher amount of expression than both sphere sizes in the high-density group (****$p < 0.0001$), while the large sphere, low density group had significantly more expression than the small sphere, high density group (*$p < 0.03$).

phenotypes, and thus lower GFAP expression, in these cultures which were not identified in this study.

Small spheres at the lower global density produced more oligodendrocytes

Maturation of NSCs into oligodendrocytes was assessed using the RIP antibody, which recognizes 2′,3′-cyclic nucleotide 3′-phosphodiesterase (CNPase) (Fig. 7a). The RIP positive area was normalized to the number of nuclei in each respective image (Fig. 7b). Global density ($p < 0.05$), sphere size ($p < 0.05$), and the interaction effects of these variables ($p < 0.001$) were statistically significant (Table S3). Significantly more oligodendrocytes were present in the small sphere size, lower global density condition than in the other three conditions. However, the large sphere size, higher global density condition was most similar to the small sphere size, lower global density condition. This indicates that the most important factor driving oligodendrocyte differentiation may be the total number of spheres, given that most RIP+ cells were found in the 1000 total spheres per hydrogel conditions.

Overall, the data indicate that average distance between spheres is the most influential factor on mNSC viability and fate

Specifically, the conditions with 1000 total spheroids had better viability than the conditions with fewer (500) or more (2000) total spheroids. This finding suggests that the 1000 total spheroid conditions strike a balance between nutrient competition and/or inadequate waste exchange, which we posit affected viability in the 2000 total spheroid conditions, and the need to maintain a sufficient cell density to provide vital paracrine signaling between spheroids.

Regardless of viability, proliferation rates (from EDU assay data) and stemness were relatively similar for all conditions evaluated, suggesting that contact-mediated growth inhibition, which likely occurs in larger spheroids, was balanced by the ability of sphere-generated growth factors and local nutrient gradients to maintain stemlike niches. However, as these data were acquired from mNSCs after 5 days in culture in differentiation medium, which lacked the mitogens needed to broadly maintain proliferation stem cells, the overall numbers of actively proliferating cells were relatively small. More dramatic differences in pluripotency maintenance may be seen for cultures with a supply of mitogens provided in the medium.

The observed strong effects of sphere size and global cell density on mNSC viability and differentiation suggests that these effects are independent of mNSC proliferation and stemness. For example, the least viable condition (2000 total spheres per hydrogel) condition also had the least neuronal cells, suggesting that higher nutrient competition might prevent differentiation. In contrast, when spheres are too sparse (*e.g.* 500 total spheres per gel) there is a more pronounced inflammatory response, indicated by the presence of $GFAP^+$ astrocytes, likely from inadequate paracrine signaling between spheres that also reduces viability. Overall, the intermediate total spheroid density conditions (1000 spheroids total) best promoted neuronal and oligodendrocyte differentiation. In general, stem cell therapies for CNS regeneration seek to

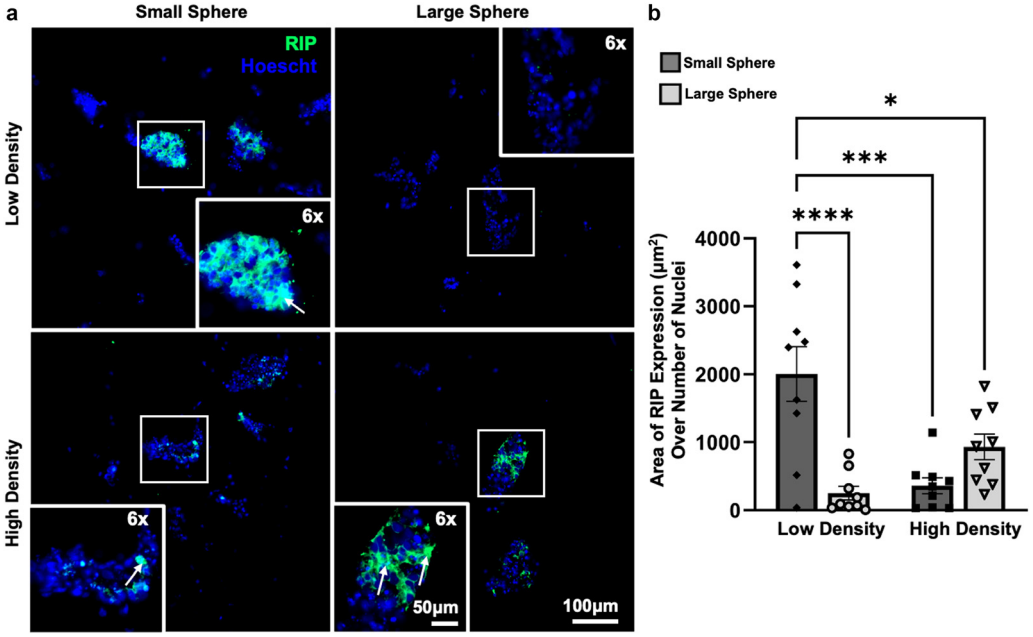

Fig. 7 On day 5 of culture in differentiation medium, the hydrogels were fixed, sectioned at 10 μm and stained for (a) RIP and Hoescht to confirm the presence of oligodendrocytes. Scale bar is 100 μm, inset scale bar is 50 μm. (b) These images were analyzed using cell profiler to determine the total area of expression divided by the number of nuclei. A test of normality (Shapiro–Wilk test) and subsequently ordinary two-way ANOVA (Tukey's multiple comparison test) was performed using GraphPad Prism to determine significance between the groups. (*$p < 0.05$, ***$p < 0.005$, ****$p < 0.0001$, $N = 9$, Error bars represent ± SEM). The small sphere, low density group had a higher amount of expression than all the other conditions.

generate new neurons and oligodendrocytes, while avoiding differentiating in astrocytes that may contribute to scarring rather than regeneration.[44]

These density-dependent effects likely reflect regulation through contact- and tension-sensitive signaling pathways that influence NSC fate. Notch signaling, which is activated by cell–cell contact, promotes stem cell maintenance and inhibits immature neuronal differentiation when local density is high.[24,25] Conversely, moderate spacing between spheroids may reduce Notch activation while enhancing Wnt/β-catenin signaling, which supports neuronal differentiation and neurite extension under lower-density conditions.[23,24] Additionally, mechanosensitive Hippo/YAP signaling is known to respond to cytoskeletal tension and cell crowding, influencing proliferation and glial lineage commitment in neural progenitors.[25] Together, these pathways provide a mechanistic basis for our observation that intermediate spheroid densities optimize both neuronal differentiation and viability by balancing Notch-mediated maintenance with Wnt- and YAP-driven maturation responses.

While neural organoids are a common approach for modeling brain-like tissue organization, they rely on self-organization processes that often lead to heterogeneous cellular composition, limited reproducibility, and diffusion constraints in the organoid core.[45] In contrast, the multi-spheroid hydrogel cultures described here enable systematic control over spheroid size, spacing, and overall density within a defined 3D microenvironment. This tunable approach allows for more reproducible studies of cell–cell and cell–matrix interactions while maintaining relevant neural cell phenotypes. Moreover, such systems may be particularly useful for applications that do not require the complex cytoarchitecture of organoids, such as high-throughput drug screening or generation of homogeneous neuronal or glial populations.[46] Similar approaches using aggregated neural spheroids have also been employed for neural tissue engineering applications to enhance cell viability, differentiation, and network formation.[15,16,27] The present study expands upon previous research to demonstrate the importance of sphere density within 3D microenvironments on neural cell survival and differentiation.

It is possible that sphere size would have larger effects if the difference in spheroid diameter investigated was greater than the 50 μm difference between the large and small spheroid diameters used in this study. However, it is important to consider reduction in oxygen transport in spheroid centers when diameters grow larger than 300 μm. In cultures with rapid cell proliferation, this size restriction is particularly important to consider as even smaller spheroids must be initially used to account for spheroid expansion.

While the 5-day studies reported here provide information about which cells are undergoing differentiation into a particular lineage, we recognize that longer culture times are required for full maturation. However, the 5-day time point is sufficient to assume that any cells expressing lineage-specific markers will continue to differentiate down this same lineage.[47] As neuronal and glial cells continue to mature and form complex synaptic networks over extended time frames, future work should investigate how long-term culture (weeks to

months) influences the structural and functional stability of these multi-spheroid systems. Extending the culture duration would provide insight into whether global culture density continues to modulate neuronal enrichment or even shifts toward specific subtypes of mature neuronal cells over time. Assessments of electrophysiological activity and network connectivity would be good indicators of maturation, at longer time points. Our future work will evaluate how culturing these multi-spheroid systems within electrically conductive hydrogels can further potentiate neuronal maturation under applied electrical stimulation. These long-term analyses will be critical to establishing the utility of this platform for modeling chronic neural processes and for applications in regenerative medicine and drug screening.

Additionally, the current study is limited by the random distribution of spheroids in 3D cultures. More precise control over the spheroid-to-spheroid distance could be achieved in future studies using bioprinting or other established methods for spheroid placement. Specifically, approaches such as aspiration bioprinting[48] and magnetic nanoparticle coating[49] can be used to more reliably spatially pattern spheroids within 3D biomaterial scaffolds and provide a clearer understanding of the effects of sphere to sphere distance.[50]

Conclusion

Our findings indicate that the density of mNSC spheroids encapsulated within 3D hydrogels strongly influences viability and differentiation. We report strong interactive effects of spheroid size and the global cell density, where conditions with intermediate spheroid densities (1000 total spheres per hydrogel) maximized viability and differentiation in neurons and oligodendrocytes. These results suggest that an intermediate spheroid density balances the need for sufficient paracrine signaling with that for adequate nutrient availability and waste exchange. While previous work has highlighted the importance of spheroid distribution, sphere size and overall cell density within 3D biomaterials independently and how this can influence viability, proliferation and migration of cells, the current study provides a truly systematic investigation of how these culture parameters affect mNSC viability and phenotype in an HA-based hydrogel platform. Importantly, these results demonstrate that total sphere density within a 3D biomaterial is at least equally as important as sphere size on viability and neuronal differentiation. This knowledge will provide future studies with a framework when designing 3D culture protocols with the goal of controlling neural stem cell fate.

Author contributions

Rebecca Duquette: methodology, investigation, resources, software, format analysis, data curation, visualization, writing – original draft preparation and creation, project administration. Sabrina-Pietrosemoli Salazar: validation, investigation, resources, writing – review and editing. Ze Zhong Wang: validation and investigation. Alireza Sohrabi: writing – review and editing. Stephanie Seidlits: conceptualization, methodology, format analysis, validation, writing – review and editing, supervision, funding.

Conflicts of interest

There are no conflicts to declare.

Data availability

Data for this article, including datasheets for all prepared data are available at figshare at https://doi.org/10.6084/m9.figshare.29493596, https://doi.org/10.6084/m9.figshare.29495405.v1, and https://doi.org/10.6084/m9.figshare.29495315.v1.

Supplementary information (SI): raw data from image quantification, flow cytometry and rheology have been provided. see DOI: https://doi.org/10.1039/d5tb01589h.

Acknowledgements

We would like to acknowledge all the members of the Seidlits Lab, in providing their valuable suggestions and feedback. We would also like to acknowledge BioRender for the creation of Fig. 1a and the Table of Contents figure in this paper.

References

1 Alzheimer's Association, 2025, Alzheimer's Disease Facts and Figures, Chicago.
2 W. Yang, J. L. Hamilton, C. Kopil, J. C. Beck, C. M. Tanner, R. L. Albin, E. Ray Dorsey, N. Dahodwala, I. Cintina, P. Hogan and T. Thompson, Current and projected future economic burden of Parkinson's disease in the U.S, *NPJ Parkinsons Dis.*, 2020, **6**, 15.
3 Y. Wang, Global, regional, and national burdens of traumatic brain injury, spinal cord injury, and skull fracture and their attributable risk factors from 1990 to 2021: a systematic analysis of the global burden of disease study 2021, *Front. Public Health*, 2025, **13**, 1622693.
4 National Spinal Cord Injury Statistical Center, *Traumatic Spinal Cord Injury Facts and Figures at a Glance*, Birmingham, 2024.
5 B. N. Kharbikar, P. Mohindra and T. A. Desai, Biomaterials to enhance stem cell transplantation, *Cell Stem Cell*, 2022, **29**(5), 692–721.
6 B. G. Ballios, M. J. Cooke, L. Donaldson, B. L. Coles, C. M. Morshead and D. van der Kooy, *et al.*, A Hyaluronan-Based Injectable Hydrogel Improves the Survival and Integration of Stem Cell Progeny following Transplantation, *Stem Cell Rep.*, 2015, **4**(6), 1031–1045.
7 Z. Giorgi, V. Veneruso, E. Petillo, P. Veglianese, G. Perale and F. Rossi, Biomaterials and Cell Therapy Combination in

Central Nervous System Treatments, *ACS Appl. Bio Mater.*, 2024, **7**(1), 80–98.

8 R. D. Bierman-Duquette, G. Safarians, J. Huang, B. Rajput, J. Y. Chen and Z. Z. Wang, *et al.*, Engineering Tissues of the Central Nervous System: Interfacing Conductive Biomaterials with Neural Stem/Progenitor Cells, *Adv. Healthcare Mater.*, 2022, **11**(7), e2101577.

9 M. Preston and L. S. Sherman, Neural stem cell niches: roles for the hyaluronan-based extracellular matrix, *Front. Biosci., Scholar Ed.*, 2011, **3**(3), 1165–1179.

10 S. K. Seidlits, J. Liang, R. D. Bierman, A. Sohrabi, J. Karam and S. M. Holley, *et al.*, Peptide-modified, hyaluronic acid-based hydrogels as a 3D culture platform for neural stem/progenitor cell engineering, *J. Biomed. Mater. Res., Part A*, 2019, **107**(4), 704–718.

11 S. K. Seidlits, Z. Z. Khaing, R. R. Petersen, J. D. Nickels, J. E. Vanscoy and J. B. Shear, *et al.*, The effects of hyaluronic acid hydrogels with tunable mechanical properties on neural progenitor cell differentiation, *Biomaterials*, 2010, **31**(14), 3930–3940.

12 M. Dovedytis, Z. J. Liu and S. Bartlett, Hyaluronic acid and its biomedical applications: A review, *Eng. Regener.*, 2020, **1**, 102–113.

13 M. T. Ho, C. J. Teal and M. S. Shoichet, A hyaluronan/methylcellulose-based hydrogel for local cell and biomolecule delivery to the central nervous system, *Brain Res. Bull.*, 2019, **148**, 46–54.

14 L. R. Nih, P. Moshayedi, I. L. Llorente, A. R. Berg, J. Cinkornpumin and W. E. Lowry, *et al.*, Engineered HA hydrogel for stem cell transplantation in the brain: Biocompatibility data using a design of experiment approach, *Data Brief*, 2017, **10**, 202–209.

15 K. H. Griffin, S. W. Fok and J. Kent Leach, Strategies to capitalize on cell spheroid therapeutic potential for tissue repair and disease modeling, *npj Regener. Med.*, 2022, **7**(1), 70.

16 A. R. Bento, P. Quelhas, M. J. Oliveira, A. P. Pego and I. F. Amaral, Three-dimensional culture of single embryonic stem-derived neural/stem progenitor cells in fibrin hydrogels: neuronal network formation and matrix remodelling, *J. Tissue Eng. Regener. Med.*, 2017, **11**(12), 3494–3507.

17 S. El Harane, S. Durual, T. Braschler, D. Andre-Levigne, N. Brembilla and K. H. Krause, *et al.*, Adipose-derived stem cell spheroids are superior to single-cell suspensions to improve fat autograft long-term survival, *J. Cell. Mol. Med.*, 2022, **26**(5), 1421–1433.

18 G. Mehta, A. Y. Hsiao, M. Ingram, G. D. Luker and S. Takayama, Opportunities and challenges for use of tumor spheroids as models to test drug delivery and efficacy, *J. Controlled Release*, 2012, **164**(2), 192–204.

19 T. Anada, J. Fukuda, Y. Sai and O. Suzuki, An oxygen-permeable spheroid culture system for the prevention of central hypoxia and necrosis of spheroids, *Biomaterials*, 2012, **33**(33), 8430–8441.

20 S. Suzuki, T. Muneta, K. Tsuji, S. Ichinose, H. Makino and A. Umezawa, *et al.*, Properties and usefulness of aggregates of synovial mesenchymal stem cells as a source for cartilage regeneration, *Arthritis Res. Ther.*, 2012, **14**(3), R136.

21 T. Distler, I. Lauria, R. Detsch, C. M. Sauter, F. Bendt and J. Kapr, *et al.*, Neuronal Differentiation from Induced Pluripotent Stem Cell-Derived Neurospheres by the Application of Oxidized Alginate-Gelatin-Laminin Hydrogels, *Biomedicines.*, 2021, **9**(3), 261.

22 Y. Lei and D. V. Schaffer, A fully defined and scalable 3D culture system for human pluripotent stem cell expansion and differentiation, *Proc. Natl. Acad. Sci. U. S. A.*, 2013, **110**(52), E5039–E5048.

23 Y. Lei, D. Jeong, J. Xiao and D. V. Schaffer, Developing Defined and Scalable 3D Culture Systems for Culturing Human Pluripotent Stem Cells at High Densities, *Cell. Mol. Bioeng.*, 2014, **7**(2), 172–183.

24 M. S. Huang, B. L. LeSavage, S. Ghorbani, A. E. Gilchrist, J. G. Roth and C. Huerta-Lopez, *et al.*, Viscoelastic N-cadherin-like interactions maintain neural progenitor cell stemness within 3D matrices, *Nat. Commun.*, 2025, **16**(1), 5213.

25 S. Rammensee, M. S. Kang, K. Georgiou, S. Kumar and D. V. Schaffer, Dynamics of Mechanosensitive Neural Stem Cell Differentiation, *Stem Cells*, 2017, **35**(2), 497–506.

26 N. D. Caprio and J. A. Burdick, Engineered biomaterials to guide spheroid formation, function, and fabrication into 3D tissue constructs, *Acta Biomater.*, 2023, **165**, 4–18.

27 S. J. Kim, H. Byun, S. Lee, E. Kim, G. M. Lee and S. J. Huh, *et al.*, Spatially arranged encapsulation of stem cell spheroids within hydrogels for the regulation of spheroid fusion and cell migration, *Acta Biomater.*, 2022, **142**, 60–72.

28 I. Pereira, M. J. Lopez-Martinez, A. Villasante, C. Introna, D. Tornero and J. M. Canals, *et al.*, Hyaluronic acid-based bioink improves the differentiation and network formation of neural progenitor cells, *Front. Bioeng. Biotechnol.*, 2023, **11**, 1110547.

29 M. P. Seitz, Y. Song, X. L. Lian, Z. Ma and E. Jain, Soft Polyethylene Glycol Hydrogels Support Human PSC Pluripotency and Morphogenesis, *ACS Biomater. Sci. Eng.*, 2024, **10**(7), 4525–4540.

30 W. Xiao, A. Ehsanipour, A. Sohrabi and S. K. Seidlits, Hyaluronic-Acid Based Hydrogels for 3-Dimensional Culture of Patient-Derived Glioblastoma Cells, *J. Visualized Exp.*, 2018, (138), e58176.

31 F. T. Zakusilo, M. Kerry O'Banion, H. A. Gelbard, A. Seluanov and V. Gorbunova, Matters of size: Roles of hyaluronan in CNS aging and disease, *Ageing Res. Rev.*, 2021, **72**, 101485.

32 J. A. W. van Dommelen, M. Hrapko and G. W. M. Peters, Mechanical Properties of Brain Tissue: Characterisation and Constitutive Modelling, *Mechanosensitivity of the Nervous System*, Springer, 2009, pp. 249–279.

33 E. P. Canovic, B. Qing, A. S. Mijailovic, A. Jagielska, M. J. Whitfield and E. Kelly, *et al.*, Characterizing Multiscale Mechanical Properties of Brain Tissue Using Atomic Force Microscopy, Impact Indentation, and Rheometry, *J. Visualized Exp.*, 2016, (115), 54201.

34 H. Mori, K. Ninomiya, M. Kino-oka, T. Shofuda, M. O. Islam and M. Yamasaki, *et al.*, Effect of neurosphere size on the growth rate of human neural stem/progenitor cells, *J. Neurosci. Res.*, 2006, **84**(8), 1682–1691.

35 R. J. McMurtrey, Analytic Models of Oxygen and Nutrient Diffusion, Metabolism Dynamics, and Architecture Optimization in Three-Dimensional Tissue Constructs with Applications and Insights in Cerebral Organoids, *Tissue Eng., Part C*, 2016, **22**(3), 221–249.

36 B. Uttara, A. V. Singh, P. Zamboni and R. T. Mahajan, Oxidative stress and neurodegenerative diseases: a review of upstream and downstream antioxidant therapeutic options, *Curr. Neuropharmacol.*, 2009, **7**(1), 65–74.

37 S. Salim, Oxidative Stress and the Central Nervous System, *J. Pharmacol. Exp. Ther.*, 2017, **360**(1), 201–205.

38 C. L. Limoli, R. Rola, E. Giedzinski, S. Mantha, T. T. Huang and J. R. Fike, Cell-density-dependent regulation of neural precursor cell function, *Proc. Natl. Acad. Sci. U. S. A.*, 2004, **101**(45), 16052–16057.

39 S. D. Ocana, D. Magaquian and C. Banchio, Neural stem cell-derived extracellular vesicles favour neuronal differentiation and plasticity under stress conditions, *Front. Mol. Neurosci.*, 2023, **16**, 1146592.

40 V. Graham, J. Khudyakov, P. Ellis and L. Pevny, SOX2 functions to maintain neural progenitor identity, *Neuron*, 2003, **39**(5), 749–765.

41 Q. Smith, E. Stukalin, S. Kusuma, S. Gerecht and S. X. Sun, Stochasticity and Spatial Interaction Govern Stem Cell Differentiation Dynamics, *Sci. Rep.*, 2015, **5**, 12617.

42 T. C. Tseng, L. Tao, F. Y. Hsieh, Y. Wei, I. M. Chiu and S. H. Hsu, An Injectable, Self-Healing Hydrogel to Repair the Central Nervous System, *Adv. Mater.*, 2015, **27**(23), 3518–3524.

43 E. M. Hol and M. Pekny, Glial fibrillary acidic protein (GFAP) and the astrocyte intermediate filament system in diseases of the central nervous system, *Curr. Opin. Cell Biol.*, 2015, **32**, 121–130.

44 J. Li, W. Luo, C. Xiao, J. Zhao, C. Xiang and W. Liu, *et al.*, Recent advances in endogenous neural stem/progenitor cell manipulation for spinal cord injury repair, *Theranostics*, 2023, **13**(12), 3966–3987.

45 Z. Zhao, X. Chen, A. M. Dowbaj, A. Sljukic, K. Bratlie and L. Lin, *et al.*, Organoids, *Nat. Rev. Methods Primers*, 2022, 2.

46 J. M. Lee, D. Y. Park, L. Yang, E. J. Kim, C. D. Ahrberg and K. B. Lee, *et al.*, Generation of uniform-sized multicellular tumor spheroids using hydrogel microwells for advanced drug screening, *Sci. Rep.*, 2018, **8**(1), 17145.

47 T. K. Kelly, S. L. Karsten, D. H. Geschwind and H. I. Kornblum, Cell lineage and regional identity of cultured spinal cord neural stem cells and comparison to brain-derived neural stem cells, *PLoS One*, 2009, **4**(1), e4213.

48 B. Ayan, D. N. Heo, Z. Zhang, M. Dey, A. Povilianskas and C. Drapaca, *et al.*, Aspiration-assisted bioprinting for precise positioning of biologics, *Sci. Adv.*, 2020, **6**(10), eaaw5111.

49 J. G. Roth, L. G. Brunel, M. S. Huang, Y. Liu, B. Cai and S. Sinha, *et al.*, Spatially controlled construction of assembloids using bioprinting, *Nat. Commun.*, 2023, **14**(1), 4346.

50 H. W. Han, Y. T. Hou and S. H. Hsu, Angiogenic potential of co-spheroids of neural stem cells and endothelial cells in injectable gelatin-based hydrogel, *Mater. Sci. Eng., C*, 2019, **99**, 140–149.